Biallelic mutations in RNF220 cause laminopathies featuring leukodystrophy, ataxia and deafness

(Article begins on next page)

11 July 2024

Biallelic mutations in *RNF220* cause laminopathies featuring leukodystrophy, ataxia and deafness

Antonella Sferra,[1] Paola Fortugno,[2,3] Marialetizia Motta,[1] Chiara Aiello,[1] Stefania Petrini,[4] Andrea Ciolfi,[1] Francesca Cipressa,[5] Isabella Moroni,[6] Vincenzo Leuzzi,[7] Luisa Pieroni,[8] Federica Marini,[9,10] Odile Boespflug Tanguy,[11,12] Eleonore Eymard-Pierre,[13] Federica Rachele Danti,[6] Claudia Compagnucci,[1] Giovanna Zambruno,[1] Alfredo Brusco,[14] Filippo M. Santorelli,[15] Luisa Chiapparini,[16] Paola Francalanci,[17] Anna Livia Loizzo,[18] Marco Tartaglia[1], Gianluca Cestra[5,8,19,†] and Enrico Bertini[1,†]

†These authors contributed equally to this work.

1 Genetics and Rare Diseases Research Division, Bambino Gesù Children's Hospital, IRCCS, 00146 Rome, Italy

2 Department of Life, Health and Environmental Sciences University of L'Aquila, 00167 Rome, Italy

3 Human Functional Genomics, IRCCS San Raffaele Pisana, 00166 Rome, Italy

4 Confocal Microscopy Core Facility, Research Laboratories, Ospedale Pediatrico Bambino Gesù, 00146 Rome, Italy

5 University of Rome "Sapienza", Department of Biology and Biotechnology, 00185 Rome, Italy

6 Department of Pediatric Neuroscience, Fondazione IRCCS Istituto Neurologico Carlo Besta, 20133 Milan, Italy

7 Department of Human Neuroscience, Unit of Child Neurology and Psychiatry, Sapienza University, 00185 Rome, Italy

8 Santa Lucia IRCCS Foundation, 00179 Rome, Italy

9 Institute of Biochemistry and Clinical Biochemistry, Università Cattolica del Sacro Cuore, 00168 Rome, Italy

10 Department of Laboratory Diagnostic and Infectious Diseases, Fondazione Policlinico Universitario Agostino Gemelli IRCCS, 00168 Rome, Italy

11 Service de Neurologie Pédiatrique, Centre de reference leucodystrophies et leucoencephalopathies de cause rare (LEUKOFRANCE), APHP Hopital Robert-Debré, 75019 Paris, France

12 Université de Paris, NeuroDiderot, UMR 1141 INSERM 75651 Paris, France

13 Service de Cytogénétique Médicale CHU de Clermont Ferrand, Hopital ESTAING 63003 CLERMONT FERRAND, France

14 Department of Medical Sciences, University of Torino, 10124 Turin, Italy

15 Molecular Medicine, IRCCS Stella Maris Foundation, 56128 Pisa, Italy

16 Neuroradiology Department, Fondazione IRCCS Istituto Neurologico Carlo Besta, 20133 Milan, Italy

17 Department of Laboratories, Pathology Unit, IRCCS Bambino Gesù Children's Hospital, 00165 Rome, Italy.

18 DIDASCO Società Cooperativa Sociale- Centro di riabilitazione, 00185 Rome, Italy

19 Institute of Molecular Biology and Pathology (IBPM), National Research Council (CNR) 00185 Rome, Italy

Abstract

Leukodystrophies are a heterogeneous group of rare inherited disorders that involve preferentially the white matter of the central nervous system (CNS). These conditions are characterized by a primary glial cell and myelin sheath pathology of variable etiology, which causes secondary axonal degeneration, generally emerging with disease progression.

Whole exome sequencing performed in 5 large consanguineous nuclear families allowed to identify homozygosity for two recurrent missense variants affecting highly conserved residues of *RNF220* as the causative event underlying a novel form of leukodystrophy with ataxia and sensorineural deafness.

We report on two homozygous missense variants (p.R363Q and p.R365Q) in the ubiquitin E3 ligase *RNF220* as the cause underlying a novel form of leukodystrophy with ataxia and sensorineural deafness having fibrotic cardiomyopathy and hepatopathy as associated features, in seven consanguineous families. Mass spectrometry analysis identified lamin B1 as RNF220 binding protein and co-immunoprecipitation experiments demonstrated reduced binding of both RNF220 mutants to lamin B1. We demonstrate that *RNF220* silencing in *Drosophila melanogaster* specifically affects proper localization of lamin Dm0, the fly lamin B1 orthologue, promotes its aggregation, and causes a neurodegenerative phenotype, strongly supporting the functional link between RNF220 and lamin B1. Finally, we demonstrate that RNF220 plays a crucial role in the maintenance of nuclear morphology: mutations primary skin fibroblasts determine nuclear abnormalities such as blebs, herniations and invaginations, which are typically observed in cells of patients affected by laminopathies.

Overall, our data identify *RNF220* as a gene implicated in leukodystrophy with ataxia and sensorineural deafness, and document a critical role of RNF220 in the regulation of nuclear lamina. Our findings provide further evidence on the direct link between nuclear lamina dysfunction and neurodegeneration.

Correspondence to: Enrico Bertini

Unit of Neuromuscular and Neurodegenerative Disorders, Genetics and Rare Diseases Research Division, Bambino Gesù Children's Hospital, IRCCS, V.le S. Paolo, 15, 00146 Rome, Italy
E-mail: bertini@opbg.net

Correspondence may also be addressed to: Antonella Sferra

E-mail: antonella.sferra@opbg.net

Running title: *RNF220* mutations in leukodystrophy

Keywords: leukodystrophy; sensorineural-deafness; fibrotic cardiomyopathy; hepatopathy; laminopathies

Abbreviations: F= female; gr= grams; h= height; l= length; M= male; ofc= occipital cranial circumpherence; w= weight ; y= years; w= weight,

Introduction

Leukodystrophies are a group of neurodegenerative diseases resulting from inherited defects of the myelin sheath formation and/or maintenance, in pyramidal and cerebellar neurons[1, 2]. They represent an important cause of progressive neurological disability in young patients. Although many forms have recognizable genetic, imaging and metabolic patterns, there are still cases running in families with unsolved etiology[3].

We report on a novel form of autosomal recessive leukodystrophy identified in seven nuclear families characterized by progressive ataxia and deafness (AR-LAD) combined with fibrotic cardiomyopathy and hepatopathy as major associated features.

Whole exome sequencing (WES) performed in 5 large consanguineous nuclear families allowed to identify homozygosity for two recurrent missense variants affecting highly conserved residues of *RNF220* as the causative event underlying AR-LAD.

RNF220 encodes an evolutionarily conserved RING finger E3 ubiquitin ligase[4] highly expressed in developing nervous system where it modulates both ventral spinal cord patterning[5-7] and cerebellum development[8]. According with its neuronal expression, RNF220 has recently been involved in the regulation of neural stem cell proliferation and differentiation[9], and in the development of noradrenergic neurons[10].

In this study, we demonstrate that RNF220 protein, which is mutated in this novel syndromic leukodystrophy AR-LAD, binds lamin B1 and plays a crucial role in the maintenance of nuclear integrity by regulating nuclear laminar proteins. Interestingly, this form of hypomyelinating leukodystrophy recalls, for some aspects, the adult-onset autosomal dominant leukodystrophy (ADLD) caused by either genomic duplications encompassing the lamin B1 gene (*LMNB1*) or deletions upstream of this gene. *LMNB1* encodes one of the major component of the nuclear lamina and all ADLD-related mutations result in increased lamin B1 protein levels in brain tissue of affected individuals[11, 12].

Overall, our findings provide new insights into RNF220 nuclear functions and its involvement in AR-LAD pathogenesis, and corroborate the implication of nuclear lamina defects in the pathogenesis of brain white matter disorders.

Materials and methods

Standard protocol approvals, registrations, and patient consent

The study was approved by the Ethical Committees of the Children Hospital Bambino Gesù, Rome, Italy in agreement with the Declaration of Helsinki. Informed consent was signed by the parents of the patients.

WES and Proteomic analysis

Detailed methods of WES analysis and Proteomic analysis are described in Supplementary Material.

Cell Culture

COS1, HEK-293T and human primary skin fibroblasts were grown in Dulbecco's modified Eagle's medium (high glucose formulation) supplemented with 10% fetal bovine serum (Thermo Fisher Scientific), 2 mM L-glutamine and 1% penicillin-streptomycin antibiotics, at 37°C in a 5% CO_2 humidified atmosphere. iPSCs were purchased from Coriell Institute

(USA, Cod GM23338, GM23340). The iPSCs were derived from human fibroblasts and reprogrammed using the episomal technology. iPSCs were differentiated into motor neurons as previously described[13].

Plasmid constructs

To generate RNF220 constructs, the entire cDNA sequence (NM-018150) was amplified from the cDNA clone MGC39525 (Thermo Scientific) and inserted into pFLAG-CMW-6a vector. RNF220 mutants were generated by site-direct mutagenesis using the QuikChange-XLII Site-Directed Mutagenesis Kit (Stratagene) according to the manufacturer's instructions**.**All the constructs were confirmed by DNA sequencing**.**

Cell transfection

Transient transfection of COS-1 and HEK-293 cells was achieved by using Lifpofectamin 2000 reagent, according to the manufacturer's instructions (Thermo Fisher Scientific). Forty-eight hours after transfection, cells were fixed or recovered for protein extraction.

Preparation of nuclear extracts and co-immunoprecipitation experiments

Preparation of nuclear extracts from transiently transfected or mock transfected HEK-293T cells was performed as previously described[14]. 400 µg of nuclear extract was incubated with 30 µl of anti-FLAG M2 antibody covalently bound to agarose beads at 4°C for 1 hour, under gently rock. After incubation, samples were centrifugated to pellet FLAG resins. After extensive washing, retained proteins were resuspended in 30 µl of Laemmli buffer, separated on SDS-PAGE and analyzed by western blotting.

Immunohistochemistry

CD1 mouse brain slices were fixed in 4% PFA at 4°C for 20 minutes, permeabilized in PBS-0.15% Triton X-100 (Sigma), blocked for 1 hour in PBS-5% BSA (Sigma) and incubated with primary antibodies at 4°C overnight. Primary antibodies were diluted in PBS-1% BSA by the following dilutions: rabbit anti RNF220 (1:50, Sigma), mouse anti Smi32 (1:500, Sigma), mouse anti Calbindin (1:500, Sigma), mouse anti GFAP (1:500, BD Biosciences). Slices were washed three times in PBS and incubated with Alexa Fluor-conjugated secondary antibodies (Thermo Fisher Scientific) for 1 hour at room temperature and nuclei were counterstained with Hoechst (Sigma).

Immunocytochemistry

Fibroblasts were seeded in 24-well cluster plates onto 12 mm cover glasses. After 24 hours of culture in complete medium, cells were fixed with ice–cold methanol for 7 minutes, blocked with PBS-5% BSA (Sigma) for 1 hour and subsequently incubated with the indicated primary

antibodies at 4°C overnight. Primary antibodies were diluted in PBS-1% BSA by the following dilutions: mouse anti Lamin AC (1:50, Santa Cruz), rabbit anti Lamin B1 (1:500, Abcam), mouse anti Nesprin-1 (MANNES1A-7A12) (1:50, Thermo Fisher Scientific)[15]. Cells were washed three times in PBS and incubated with Alexa Fluor-conjugated secondary antibodies (Thermo Fisher Scientific) for 1 hour at room temperature. Nuclei were counterstained with Hoechst (Sigma).

COS-1 cells transiently transfected were fixed in 4% PFA for 15 minutes, blocked with PBS-5% BSA (Sigma) for 1 hour and subsequently incubated with the primary mouse anti FLAG antibody (1:500, Sigma) for 1 hour at room temperature or with the indicated primary antibodies at 4°C overnight: rabbit anti 20S Proteasome (1:100, Thermo Fisher Scientific) rabbit anti ASF/SF2 (1:100, Abcam). Cells were washed three times in PBS and incubated with Alexa Fluor-conjugated secondary antibodies (Thermo Fisher Scientific) for 1 hour at room temperature. Nuclei were Hoechst (Sigma) counterstained.

Confocal microscopy analysis

Confocal imaging was performed on an Olympus Fluoview FV1000 confocal microscope equipped with Multi Ar (458–488 and 515 nm), 2X He/Ne (543 and 633 nm), and 405-nm diode lasers. Sequential confocal images were acquired using a HC PLAPO CS2 40× oil-immersion objective with a 1024×1024 format, 400 Hz scan speed and a z-step size of 0.4 μm. The lasers' power, beam splitters, filter settings, pinhole diameter and scan mode were the same for all examined samples of each staining. The spatial relationship between RNF220 and 20S proteasome was quantified by co-localization analysis module of LAS X Leica software, using Manders' Overlap Coefficient (OC). Its value can range from 0 to 1, with 0 represents a total exclusion, 0,5 a random overlap, and 1 reflecting 100% co-localization between both images. The co-localization is considered significant when OC>0.5.

Drosophila strains and crosses

Flies stocks were maintained on Drosophila standard medium (Nutri-fly Genesee Scientific) at 25°C and crosses were performed at 18 and 25°C. RNF220 down regulation in different tissues was obtained by crossing UAS RNF220 RNAi (BDSC 61303) with Eyeless-GAL4 (eye imaginal disc and larval salivary glands), GMR-GAL4 (adult eye) or Mef2-GAL4 (larval muscles) flies. All stocks were provided by Bloomington Stock Center and described in flybase.org.

Drosophila salivary glands immunostaining

Third instar larval salivary glands were dissected in 0.7% NaCl, transferred in 1.8% formaldehyde and 40% acetic acid on a coverslip, gently squashed and immediately frozen in

liquid nitrogen. After flipping off the coverslip, slides were immersed in ice cold TBS for 10 minutes and permeabilized for 20 minutes in TBS-Triton 1%. Slides were then incubated with anti Lamin Dm0 (1:10; ADL67.10-S Developmental Studies Hybridoma Bank) and Anti Lamin C (1:10; LC28.26-S Developmental Studies Hybridoma Bank) antibodies overnight at 4°C in a wet chamber. Salivary glands preparations were washed 10 minutes with TBS-Triton 0,05% and incubated with anti-mouse TRITC (Jackson Immuno Research) 1 hour at room temperature. After two washes with TBS-Triton 0,05%, slides were mounted in VECTASHIELD Antifade Mounting Medium with DAPI (Vector) to stain DNA. Intact polytene chromosomes nuclei were analyzed using a Zeiss Axioplan epifluorescence microscope (Carl Zeiss) equipped with a cooled CCD camera (Photometrics). Images were pseudo coloured and merged with Adobe Photoshop CS4.

RNA extraction, cDNA synthetis, Real-Time PCR and PCR

Total RNA from UAS-RNF220-RNAi/Mef2 GAL4 and control +/Mef2 GAL4 were extracted from third instar larvae (2 larvae/sample) using Nucleozol (Macherey Nagel) by following the manufacturer's manual and genomic DNA was digested with InvitrogenTM Dnase I Amplification Grade (Thermo Fisher Scientific). 400 ng of each total RNA were retrotranscribed into equal amount of cDNA by using the iScript™ cDNA Synthesis Kit (Bio-Rad) and 35 ng of cDNA for each reaction were amplified in a quantitative Real-Time PCR using SsoAdvanced™ Universal SYBR® Green Supermix kit (Bio-Rad) according to the manufacturer's protocol.

Total RNA from skin fibroblasts of patients and healthy individuals were isolated using the Total RNA Purification Plus kit (Norgen Biotek Corp), according to the manufacturer's protocol. 500 ng of each RNA samples was reverse transcribed with the LunaScript RT SuperMix Kit (Euroclone) and 25 ng of cDNA for each reaction were amplified in a quantitative Real-Time PCR using Power SYBR Green PCR Master Mix (Thermo Fisher Scientific).

RNF220 splice variants were amplified using 25 ng of cDNA obtained from skin fibroblast of patients and healthy individuals and a commercial total human brain (Takara BIO) using the KAPA Taq PCR Kit (Roche).

The determination of the expression levels of the RNF220 mRNA in a commercially available human cDNA panels from healthy adult tissues (Takara BIO) and fetal brain areas (BioChain, Newark, CA) was analyzed by quantitative Real-time PCR using two inventoried TaqMan®-MBP probes (Thermo Fisher Scientific).

Data analysis and Statistics

Results are presented as the mean ± standard error of the mean (SEM). The statistical analysis was performed using the GRAPHPAD/Prism 7.0 Software (GraphPad Software). Statistically significant differences between groups were analyzed using the Student's t-test for normally distributed variables. Statistical significance was defined as * $p \leq 0.05$, ** $p \leq 0.005$, *** $p \leq 0.0005$,**** $p \leq 0.0001$.

Data availability

LC-MS raw data (e.g. mass spectra) have not been shared because they would need specific software to be visualized, but are available upon request. The data we shared (Supplementary Table 3) are representative of raw data processing.

Results

Patients and genomic analyses

We studied by WES a trio from a consanguineous nuclear family of Roma ethnicity originating from Croatia (family pedigree 2) (Fig. 1A). In this family, 3 sibs were affected by a similar early-onset hypomyelinating leukodystrophy, having progressive ataxia, sensorineural deafness, fibrotic cardiomyopathy and hepatopathy as major associated features. Cardiac manifestations progressed to dilated cardiomyopathy that caused their death by the end of the first decade (Table 1, Supplementary file). The proband pt I, 3 had been enrolled in the "Undiagnosed Patients Program", Ospedale Pediatrico Bambino Gesù, Rome. WES analysis excluded the occurrence of any functionally relevant variant (s) compatible with known Mendelian disorders based on the expected inheritance model and clinical presentation. Our variant filtering and prioritization strategy lead us to identify 8 genes carrying putative deleterious biallelic variants as the best candidates underlying the trait (Supplementary Table 1). A following analysis taking advantage of gnomAD's gene constraint metrics[16] highlighted that *RNF220* (MIM 616136) has by far the highest probability of being loss-of-function intolerant (pLI =1, observed-to-expected ratio (o/e)=0.03-0.2) in the gene. Moreover, a bioinformatic analysis showed that Arg365 is intolerant to missense variants (MetaDome's tolerance score (dn/ds) = 0.51; Supplementary Fig. 1;[17]). Overall, *RNF220* (NM_018150.4:c.1094G>A, p.(R365Q), with a CADD score of 25.8 was identified as the only putative candidate fitting the recessive transmission of the trait and homozygosity by descent. Co-segregation analysis confirmed homozygosity for the missense change in the other two affected sibs as well as heterozygosity in the two obligate

carriers and in 4 healthy sibs. We also annotated this variant in population genetics databases, with MAF<0.01 (dbSNP: rs1010750511; maximum AF in a gnomAD subpopulation = 0.0001202, with no homozygous individuals reported).

Three nuclear related families of a large consanguineous pedigree originating from southern Italy were identified to transmit a superimposed phenotype characterized by ataxia, deafness, hypomyelinating leukodystrophy, and fatal cardiomyopathy together with hepatopathy that was detected in the clinical follow-up[18]. Homozygosity mapping including the 3 AR-LAD affected patients, 6 healthy sibs and four relatives (for pedigree see Leuzzi *et al.,* 2000[18]), defined a likely region of homozygosity on chromosome 1p34.3-p33 encompassing the *RNF220* gene. Based on the clinical overlap, scan of the entire *RNF220* coding sequence allowed to identify a second missense change affecting an adjacent residue (c.1088G>A; p.(R363Q)) that co-segregated as homozygous change with the trait. This mutation c.1088G>A, with a CADD score of 32, was heterozygous in 6 additional healthy sibs and 4 relatives. It was annotated in the reference scientific databases with MAF<0.01 (dbSNP: rs780921270; maximum AF in a gnomAD subpopulation = 0.000054 and no homozygotes reported, dn/ds = 0.54) (Supplementary Fig.1).

Finally, by Genematcher imputation, additional 7 affected subjects from 3 large Roma pedigrees (Fig. 1A) sharing an overlapping neurodegenerative disorder and homozygosity for the previously recognised c.1094G>A; (p.R365Q) substitution were identified. Interestingly, multiple sequence alignments performed with ClustalW showed that both missense variants, p.R363Q and p.R365Q, target evolutionary conserved residues (Fig. 1B). Genotyping for single nucleotide polymorphisms (SNPs) opportunely selected within the homozygous genomic region encompassing *RNF220* from affected and apparently unrelated Roma subjects (Pedigree 2, 3 and 4) showed a shared haplotype indicating a founder effect (Supplementary Table 2).

Clinical features of patients are schematically listed in Table 1 and their clinical reports are summarized in the Supplemental File (Case Report). Most of the patients died during the follow up, and the main cause of death occurred after the appearance of a cardiomyopathy. Remarkably, all patients belonging to the Roma ethnicity harbouring the homozygous p.R365Q variant died around the end of the first decade, while patients originating from the southern Italian pedigree, carrying the homozygous p.R363Q, deceased by the end of the second decade.

Neuroimages showed a recognizable distribution of hypomyelination that diffusely involves the white matter of the brain, and spares the white matter of the cerebellum (Fig. 2). Of note,

T2 and Flair hyperintensity was particularly enhanced at the level of the periventricular anterior and posterior areas.

Histological analysis of the autopsy heart sample and liver biopsy from patients showed significant alterations (Supplementary Fig. 2). Heart sample from autopsy of the 18 year old patient 3, pedigree 1[18] showed replacement of myofiber by fibrotic tissue associated to a prominent interstitial fibrosis (Supplementary Fig. 2A). Similarly, liver samples from an open biopsy of I,3 in pedigree 2 (Fig. 1A) showed bridging portal fibrotic septa with chronic inflammation and parenchymal congestion and atrophy (Supplementary Fig. 2C). More interestingly, histopathological analysis of the brain samples from autopsy performed on patient 3 in pedigree 1[18] showed microvacuolar changes of the neuropile (Supplementary Fig. 3A and B), with no effects on astrocyte proliferation, or axonal spheroids (Supplementary Fig. 3A and B). Moreover, Luxol fast blu staining, to label myelin in the white matter, showed severe hypomyelination and diffuse gliosis, when compared to a control (Supplementary Fig. 3E and F).

RNF220 tissue expression profile and its localization in central nervous system

We assessed *RNF220* tissue expression profile using a commercial cDNA panel from different human adult tissues (Supplementary Fig. 4A). In accord with the expression data deposited in public database (GTEX, BioGPS and SAGE), qRT-PCR analysis revealed an ubiquitous expression of *RNF220*, which is abundant in brain and spinal cord, and particularly in cerebellum and cerebral cortex (Supplementary Fig. 4A). We also determined *RNF220* mRNA levels in human foetal CNS, observing a higher expression in the cerebellum, spinal cord and cortex (Supplementary Fig. 4B). Furthermore, we investigated the distribution of RNF220 protein in mouse CNS (8 day-old mouse). To this aim, we conducted immunofluorescence studies on hippocampus, cerebellum and telencephalon of mouse brain by using a polyclonal antibody against RNF220 in combination with neural and glial cell markers (GFAP, Nestin, Smi32 and Calbindin). A basal expression of RNF220 was observed in hippocampus and telencephalon, while a prominent localization was appreciated in the cerebellum. In the dentate gyrus of hippocampus RNF220 was poorly detected, while it was predominantly observed in the molecular layer of CA1, CA2 and CA3 regions (Fig. 3). In telencephalon and cerebellum, RNF220 staining was detected in mature neurons that express the neuronal marker Smi32 (Fig. 3). Conversely, no immunoreactivity of RNF220 was detected in astro-glial cells that are immune-reactive for GFAP, or in neural progenitor cells, which are identified by the expression of Nestin (Fig. 3). In particular, RNF220 was

widely expressed in the cerebellum where it was detected in the external granular layer, in deep cerebellar nuclei and in Purkinje cells, these last specifically labelled by the anti-Calbindin antibody (Fig. 3). Further, while RNF220 in hippocampus and telencephalon showed a predominantly cytoplasmic and perinuclear localization, it localized primarily to the nucleus in cerebellar neurons (Fig. 3).

To further characterize the expression pattern of RNF220 in neuronal cells we investigated RNF220 localization at different stages of *in vitro* differentiation of human iPSC into motor neurons. As shown in Supplementary Fig. 5, at Day 0, RNF220 staining is weak and has a widespread cytosolic distribution, while at Day 5, when first neurons appear, RNF220 staining greatly increases and localizes into the nucleus, according to the subcellular localization reported in the Human Protein Atlas. RNF220 localization remains clearly nuclear from Day 10 to Day 25 of *in vitro* differentiation. However, at Day 30, when differentiation is complete and motor neurons are mature, showing clearly defined axons and dendrites, RNF220 is widely distributed among nucleus and neurites (Supplementary Fig. 5).

Subcellular localization of RNF220 proteins in cell lines

In order to characterize the subcellular localization of wild type and mutant RNF220 we subcloned *RNF220* cDNA in different expression vectors. Firstly, we demonstrated that the subcellular distribution of RNF220 was not affected by tag positioning (Supplementary Fig. 6A). Thus, we observed in COS-1 cells transiently transfected with pFLAG-CMV-6a vector encoding N-terminal FLAG-tagged RNF220 (WT and mutants), that RNF220 localizes primarily to the nucleus (Supplementary Fig. 6A), consistently with previous findings reported in HEK-293T transfected cells[6]. In the nucleus, RNF220 labels vesicle-like structures with a distribution that strongly recalls nuclear speckles, dynamic interchromatin clusters enriched in splicing factors, which continuously exchange factors with the nucleoplasm and transcriptionally active regions[19]. Recent reports describe that proteasomal-mediated protein degradation in the nucleus occurs in distinct nucleoplasmic foci, which partially overlap with nuclear speckles[20], promyelocytic leukemia bodies (PML)[21] and clustosomes[22]. To assess whether RNF220 vesicle-like structures colocalize with nuclear speckles, cells ectopically expressing wild type RNF220 were labelled, in co-immunofluorescence experiments, with the antibody against ASF/SF2, a splicing factor enriched in nuclear speckles (Supplementary Fig. 6B). As shown, RNF220 significantly co-localizes with ASF2/SF2, suggesting that RNF220 is enriched in nuclear speckles (Supplementary Fig. 6B). Furthermore, we explored the relationship between RNF220 and the ubiquitin proteasome system (UPS) in COS1-cells, by analyzing in immunofluorescence

experiments, RNF220 co-localization with the 20S protein complex, the catalytic core of the 26S proteasome. The spatial relationship between RNF220 and 20S proteasome, examined by co-localization analysis of their confocal images, detected a partial co-distribution degree, thus suggesting a moderate link between the two molecules (Supplementary Fig. 6C). Whilst wild type RNF220 rarely forms vesicle-like structures in the cytoplasm, we observed that RNF220 mutant proteins (both RNF220_R363Q and RNF220_R365Q) localize not only in nuclear speckles, but also coalesce in the cytoplasm to form protein aggregates/inclusions (Fig. 4). This was confirmed by localizing RNF220 by immunofluorescence in patient's primary fibroblasts, showing increased signal, with abnormal increase in the cytoplasm with increased immunofluorescence for 20S proteasome as well (Fig. 5).

Proteomic identification of RNF220 interacting proteins

To gain further insight into the cellular functions of RNF220, a proteomic analysis was performed to identify RNF220 interactors. The total lysates obtained from HEK-293T cells, either non transfected (mock fraction) or expressing FLAG tagged wild type RNF220, were immunoprecipitated using anti-FLAG monoclonal antibody covalently linked to sepharose beads to isolate RNF220 and its binding partners. Proteins retained by RNF220 were separated by SDS-PAGE, purified, and identified by liquid chromatography-tandem mass spectrometry. Proteins retained by RNF220, but absent in the mock fraction, are listed in Supplementary Table 2 . Considering the nuclear localization of RNF220, we focused our attention on nuclear candidate proteins (Supplementary Fig. 7). Among the putative nuclear interactors, an enrichment of all members of the lamin protein family (i.e., lamin B1, lamin AC and lamin B2) was observed, suggesting a potential role of RNF220 in the functional regulation of lamin proteins.

RNAi-mediated downregulation of *Drosophila RNF220* specifically affects lamin B1 fly orthologue and causes neurodegeneration

To address a potential role of RNF220 in lamin protein regulation, we evaluated the effect of *RNF220* silencing on fly orthologues of lamin protein family, by downregulating *RNF220* expression in *Drosophila* tissues through the UAS-GAL4 system. Firstly, we verified by RT-qPCR that the expression of a specific *RNF220* RNAi construct in larval muscles under control of Mef2-GAL4 driver at 18°C, downregulates *RNF220* expression (Fig. 5A). Interestingly, the same RNAi construct causes adult fly lethality when expressed in larval muscles at 25°C. Further, we observed that RNAi-mediated downregulation of *RNF220* late during eye development, under GMR-GAL4 at 25°C, causes a striking neurodegeneration of the retina (Fig. 5B, upper panel). Moreover, repression of *RNF220* early during fly eye and

salivary gland development at 25°C, under control of eyeless-GAL4, causes adult fly lethality. Moreover, the same flies grown at the lower temperature of 18°C, which reduces RNAi expression, show severe alterations of eye development linked to significant reduction of eye surface (Fig. 5B, lower panel). Finally, to assess the effects of *RNF220* downregulation on the localization of fly orthologue of lamin protein family, we prepared salivary gland cells from fly larvae expressing *RNF220* RNAi under eyeless-GAL4, at 25°C. Although these conditions cause adult lethality, they are compatible with larval development. *RNF220* repression in fly salivary gland cells significantly and specifically alters the subcellular localization of lamin Dm0, the fly orthologue of human lamin B1, and promotes its accumulation (Fig. 5C). Interestingly, no effect was observed on the subcellular localization and expression levels of fly orthologue of lamin A/C (lamin C), in the same preparation (Fig. 5D).

AR-LAD mutations affect RNF220 binding activity for lamin B1

Based on the interactome data and the specific impact of *RNF220* silencing on localization and accumulation of the fly ortholog of lamin B1, we investigated the association of endogenous RNF220 and lamin B1 by subcellular fractionation and co-immunoprecipitation experiments. Firstly, we compared the distribution of RNF-220 and lamin B1 in subcellular fractions of nuclei from mouse cerebellum (Supplementary Fig. 9A), which showed high expression of RNF220 (Fig. 3). Interestingly, RNF220 and Lamin B1 show a very similar distribution with a substantial enriched in the nuclear matrix fraction, which contains a very low amount of total proteins (Supplementary Fig. 9A). Thus, we immunoprecipated Lamin B1 from solubilized proteins extracted from the nuclear matrix of cerebellar cells and we demonstrated a significant interaction of endogenous lamin B1 with RNF220 (Fig. 6A). Furthermore, to assess how the mutations affect RNF220 binding activity to lamin B1 we performed co-immunoprecipitation experiments on nuclear lysates from HEK-293T cells transfected with RNF220 constructs. .Thus, we observed that both RNF220 mutants show reduced binding to endogenous lamin B1 as compared to WT (Fig. 6B). Reduction was particularly evident if we normalize the amount of retained lamin B1 for the correspondent level of each immunoprecipitated RNF220 variant (Fig. 6B). Interestingly, p.R365Q substitution affects lamin B1 binding more seriously as compared to p.R363Q mutation (Fig. 6B).

To get insights on the molecular mechanisms underlying the role of RNF220 on the regulation of lamin B1, we assessed the effects of RNF220 expression on lamin B1 stability and ubiquitination in nuclear extracts. Since it has been already established as lamin B1 can

be degraded through ubiquitin-proteasome pathways[23] as well as via autophagy[24], we co-expressed RNF220 and lamin B1 with tagged ubiquitin with or without Bafilomycin, a lysosomal inhibitor which specifically blocks the autophagy flux (Supplementary Fig. 9B). Thus, although lamin B1 is ubiquitinated in the absence of RNF220, its ubiquitination increases in the presence of RNF220 WT, and more intriguingly, RNF220 mutants significantly reduce the ubiquitination of nuclear Lamin B1 (Supplementary Fig. 9B). Noticeable, such effect is evidenced by the treatment of Bafilomycin suggesting a role of RNF220 on both ubiquitination and autophagy processes (Supplementary Fig. 9B).

p.R363Q and p.R365Q mutations affect nuclear lamina morphology of fibroblasts

Considering the nuclear localization of RNF220, its binding to lamin B1, one of the major component of the nuclear lamina, and the effects of *RNF220* downregulation in Drosophila, we assessed the effects of *RNF220* mutations on the morphology of nuclear envelop in AR-LAD skin fibroblasts. Firstly, we verified fibroblasts as valuable system to model AR-LAD, by evaluating the expression level of *RNF220* in these cells. Evidence from the EST database suggests the presence of at least six alternatively splice variants of *RNF220* mRNA, three of which RNF220-202/203/204 (ENST00000355387, ENST00000361799, ENST00000372247) that encode full length protein and the three additional splice variants RNF220-201 (ENST00000335497), RNF220-205 (ENST00000440132) and RNF220-206 (ENST00000453863), encoding for shorter isoforms. Specific primer pairs able to detect all transcripts were exploited in RT-qPCR experiments from AR-LAD and control skin fibroblasts (Supplementary Fig. 8A). As shown in Supplementary Fig. 8B, RT-qPCR analysis showed the expression of different *RNF220* variants in primary fibroblast culture. Specifically, while variants 201, 205 and 206 were amplified in fibroblasts, the full length variants were not detected in these cells, according to their brain specific expression (Supplementary Fig. 8B). Furthermore, we assessed the expression of the different spliced variants in fibroblasts of healthy and AR-LAD affected individuals, and we confirmed that variants 201, 205 and 206 are expressed in all genetic backgrounds. Thus, although *RNF220* full length variant is not expressed, other isoforms containing the protein domains carrying AR-LAD mutations are expressed in fibroblasts.

Confocal analysis of AR-LAD fibroblasts, immunostained with different nuclear envelope markers, shows abnormal nuclear shapes in patient cells, significantly more frequent than controls, with multiple invaginations and lobulations (Fig.7).

Discussion

Here, we describe a rare form of hypomyelinating leukodystrophy manifesting as progressive ataxia, mild intellectual disability, and deafness. As disease progresses, patients experience sensory-neural deafness, resulting in complete hearing loss by their first decade of life. Moreover, during the follow-up most patients show signs of hepatopathy with increased AST (aspartate aminotransferase) and ALT (alanine aminotransferase), which is associated with periportal fibrosis at liver biopsy. Most importantly, all patients during the late follow-up develop a fatal cardiomyopathy that leads to death by the end of the second decade. Following the peculiar clinical and neuroradiological characteristics, we define this new type of white matter disease as a novel form of leukodystrophy with autosomal recessive pattern of inheritance and associated with ataxia and deafness (AR-LAD). The MRI in patients affected by AR-LAD corresponds to a hypomyelinating leukodystrophy that diffusely involves the entire white matter including the subcortical U fibers and the internal capsule, with abnormal T2 hyperintensity that is particularly enhanced at the level of the periventricular areas (Fig. 3). Moreover, hypomyelination characteristically spares the cerebellar and the brainstem white matter (Fig. 3). The distribution of hypomyelination differs from the one described in ADLD related to *LMNB1* duplication where T2 symmetric diffuse hyperintensities generally spare U-fibers as well as the periventricular white matter in the brain, and involve the upper and middle cerebellar peduncles[25].

WES analysis allowed us to identify *RNF220* as the AR-LAD causative gene, and two different homozygous mutations in two highly conserved and close residues (Fig. 1B) in exon 8, c.1088G>A (p.R363Q) and c.1094G>A (p.R365Q), were identified in AR-LAD patients. In the Roma families, we demonstrated a founder effect of the p.R365Q mutation, for which we did not find any homozygosity in the major control general population database (gnomAD), although genomic databases limited to Roma population are not available so far. The phenotype-genotype correlation shows that individuals carrying the biallelic p.R365Q mutation are more severely affected and die around the end of the first decade, only few years after the onset of cardiomyopathy, while subjects harboring the homozygous p.R363Q mutation survive until the end of the second decade, according to the later onset of cardiomyopathy. Although we have not completely elucidated the reasons for this difference, it is interesting to notice that the loss of binding activity of p.R365Q mutant to lamin B1 and its propensity to form cytoplasmic aggregations are more exacerbated that the p.R363Q

mutant. Intriguingly, these mutations show comparatively also different activity on lamin B1 in the in vitro ubiquitination assay (Supplementary Fig. 9B).

RNF220 has been previously described as a RING finger protein with E3 ubiquitin ligase activity[4] which is highly expressed in developing mouse nervous system[5, 6], and is involved by modulating the Sonic hedgehog/GLI signalling, in ventral spinal cord patterning [5, 6] and cerebellum development[8]. E3 ubiquitin ligases are key components of the UPS, one of the major cellular routes to eliminate misfolded proteins[26, 27], and catalyze the covalent attachment of one or more ubiquitin moiety to their target proteins. These modifications exert diverse effects, ranging from proteasome-dependent proteolysis to post translational modifications that modulate protein function, structural conformation and subcellular localization[28-31].

Consistent with previous studies[5, 6, 8], we observed a widespread expression of RNF220 in mouse central nervous system, with a predominant localization in the cerebellum: in the external granular layer, deep cerebellar nuclei and Purkinje cells (Fig. 4). Moreover, according to its reported role in the mouse spinal cord, and cerebellum pattern formation[5, 6, 8], we also detected high expression levels of human *RNF220* mRNA in fetal and adult spinal cord, and cerebellum (Supplementary Fig. 4).

In order to characterize the effect of AR-LAD-linked mutations on the subcellular localization of RNF220 we expressed wild type and mutant RNF220 variants in COS-1 cells and we observed their preferential nuclear localization (Supplementary Fig. 6A). We showed that wild type RNF220 protein mainly localizes in the nuclear speckles as demonstrated by the co-localization with ASF/SF2 (Supplementary Fig. 6B). Interestingly, nuclear speckles, beside their well-known role of interchromatin clusters enriched in pre-mRNA splicing factors, are likely involved in protein degradation *via* UPS[20]. Accordingly, we observed also a co-localization of RNF220 positive nuclear speckles with the 20S proteasome complex although was not highly significant (Supplementary Fig. 6C). RNF220 carrying p.R363Q and p.R365Q mutations do not localize exclusively in nuclear speckles, but also coalesces into the cytoplasm to form protein inclusions. This observation strongly suggests that AR-LAD mutations affect RNF220 subcellular localization and increase its cytoplasmic aggregation (Fig. 5).

We used a proteomic-based approach to identify RNF220 binding partners. Mass spectrometry analysis detected, among RNF220 nuclear binding proteins, all components of lamin protein family: lamin B1, lamin AC and lamin B2 (Supplementary Fig. 7). By RNAi-mediated downregulation of *RNF220* in different fly tissues we demonstrated that *RNF220*

silencing affects the subcellular localization of lamin Dm0, the fly orthologue of lamin B1, promoting its aggregation and neurodegeneration (Fig. 5). Further, *RNF220* silencing does not affect the subcellular localization of fly orthologue of lamin A/C, suggesting that *RNF220* dysregulation primarily targets lamin B1. Thus, we validated, by co-immunoprecipitation experiments, RNF220 and lamin B1 protein association and we demonstrated that AR-LAD mutations, particularly p.R365Q, significantly diminish RNF220 binding to lamin B1..

Lamin B1, encoded by the *LMNB1* gene, is a member of the intermediate filament protein family and is part of the nuclear lamina, the protein meshwork lining the inner surface of the nuclear envelope[32, 33]. Nuclear lamina not only provides mechanical support to the nucleus, but also plays a dynamic role in the organization and regulation of chromatin, transcription, DNA replication, DNA repair and epigenetic modifications[34-40]. Lamin B1 is critical for proper brain development[41-45] and the entire CNS is susceptible to modifications of *LMNB1* levels[11, 12, 46-48]. Duplication of *LMNB1* or a large deletion of 660kb upstream this gene, which dysregulate the *LMNB1* gene dosage in brain tissue, have been reported to cause a severe progressive demyelinating disorder represented by an adult form of dominant leukodystrophy (ADLD)[11, 12, 48-51]. ADLD patients exhibit increased levels of lamin B1 transcript and protein in specific degenerating cerebral area, indicating that abnormal levels of lamin B1 have deleterious consequences[11, 12]. Interestingly, AR-LAD hypomyelination reminds the deficiency in myelin deposition observed in ADLD, and suggests that the reduced interaction of RNF220 with lamin B1 may selectively affect oligodendrocytes, and neurons which are the most sensitive cells to lamin B1 dysregulation[11, 52-58]. Indeed, it has been observed that lamin B1 overexpression in oligodendrocytes leads to a premature differentiation arrest and suppression of myelin biosynthesis[53]. Accordingly, lamin B1 is tightly regulated during brain development, showing an expression pattern complementary to that of several myelin proteins[55], and particularly oligodendrocyte differentiation is characterized by a progressive decline of lamin B1 expression[58]. Furthermore, lamin B1 levels vary during neurogenesis[59, 60] and differentially regulate axon and dendrite outgrowth[58]. This tight modulation of lamin B1 protein dosage implies the involvement of specific regulatory mechanisms. Recent studies have highlighted an important role of UPS in lamin B1 turnover[61-63] and different E3 ligases, such as RNF123 and HECW2, have been reported to bind and target lamin B1 for proteasome proteolysis[61, 62]. Moreover, overexpression of human lamin B1 in Drosophila eyes causes a retina neurodegeneration[11] that strongly resembles the phenotype observed in flies expressing *RNF220* RNAi construct (Fig. 5). According to the nuclear localization of RNF220, and its functional connection with

lamin B1, we investigated the impact of RNF220 mutations on nuclear lamina morphology in AR-LAD primary fibroblasts. Morphological analysis of nuclear envelope in AR-LAD fibroblasts reveals a higher frequency of blebs, herniations and honeycomb structures, which are typically observed in laminopathic patient cells (Fig. 7). These findings confirm the involvement of RNF220 in the maintenance of nuclear integrity and allow to hypothesize that the cardiomyopathy developed by the patients may be related to a secondary laminopathy.

Indeed the fatal dilated cardiomyopathy with diffuse fibrosis seen in AR-LAD is suggestive of the cardiomyopathy observed in patients affected by laminopathies[64-66]. Laminopathic patients harbor mutations in the *LMNA* gene, encoding A-type lamins (Lamin A-C), two structural components of the nuclear lamina, or in other genes encoding proteins functionally related to lamin A-C[67].

Therefore, in the light of these pieces of evidence we cannot exclude that RNF220 mutations may impair its binding to additional lamins and that other laminar proteins may contribute to the morphological alterations observed in AR-LAD cells. Indeed, several indications link, directly or indirectly, laminopathies to an impairment of UPS[68-70]. Specific components of the UPS are activated by lamin miss-expression[68,71,72] and clearance of the inner nuclear membrane proteins have been reported to be proteasome-mediated[73,74]. Furthermore, some deleterious mutations of the lamin A-C proteins specifically affect their interaction with ubiquitin E3 ligases[62, 72, 75]. It has also reported that components of nuclear lamina are degraded by the autophagy machinery through a direct interaction of lamin B1 with LC3, a major regulator of autophagy, in a specific transport from nucleus to cytoplasm which ends with lysosomal degradation[24].

Unfortunately we had no direct access to any affected post-mitotic tissue of patients, such as the brain, which is the tissue mainly affected by AR-LAD leukodystrophy, to verify a possible accumulation of lamin proteins in degenerating cerebral areas. Although the absence of patient's autoptic tissues represent a great limitation, our *in vitro* and *in vivo* experiments strongly support the involvement of RNF220 in lamin B1 and potentially other lamin proteins turnover.

Finally, mutations in genes encoding proteins of the linker of nucleoskeleton and cytoskeleton (LINC) complex, that associate nuclear lamina to the cytoskeleton, have been reported to cause hereditary hearing loss[77, 78]. In mice deficient in structural proteins of the LINC complex outer hair fail to maintain the basal localization of their nuclei and degenerate as hearing matures[76, 77]. Considering that all AR-LAD patients experienced sensory-neural

deafness resulting in complete hearing loss within the first decade, it is captivating to hypothesize that alterations of nuclear lamina in AR-LAD cells may impair its connection with the cytoskeleton *via* the LINC complex, causing hearing loss. Accordingly, it has also been recently observed in Drosophila that mutations in the Parkin-like E3 ubiquitin ligase Ariadne-1, which regulates LINC complex, alter nuclear morphology of larval muscles, and that rare variants of human homolog of this gene are associated with thoracic aortic aneurysms due to aberrant nuclear envelop function in smooth muscle cell[78].

Overall, our findings shed new lights on RNF220 nuclear functions and strongly suggest that RNF220 may play a key role in the maintenance of nuclear integrity by regulating laminar proteins.

Acknowledgements

Funding

Competing interests

The authors report no competing interests.'

Supplementary material

Supplementary material is available at *Brain* online.

References

1. van der Knaap MS, Bugiani M. Leukodystrophies: a proposed classification system based on pathological changes and pathogenetic mechanisms. [Review]. Acta Neuropathol 2017; 134: 351-382.

2. Lin DS, Ho CS, Huang YW, Wu TY, Lee TH, Huang ZD, et al. Impairment of Proteasome and Autophagy Underlying the Pathogenesis of Leukodystrophy. Cells 2020; 1: 9:1124

3. Kohlschütter A, Eichler F. Childhood leukodystrophies: a clinical perspective. [Review]. Expert Rev Neurother 2011; 11: 1485-96.

4. Kong Q, Zeng W, Wu J, Hu W, Li C, Mao B. RNF220, an E3 ubiquitin ligase that targets Sin3B for ubiquitination. Biochem Biophys Res Commun 2010; 19; 393: 708-713.

5. Kim J, Choi TI, Park S, Kim MH, Kim CH, Lee S. Rnf220 cooperates with Zc4h2 to specify spinal progenitor domains. Development 2018; 3; 145: dev165340.

6. Ma P, Song NN, Li Y, Zhang Q, Zhang L, Zhang L, et al. Fine-Tuning of Shh/Gli Signaling Gradient by Non-proteolytic Ubiquitination during Neural Patterning. Cell Rep 2019; 28: 541-53.e4.

7. Ma P, Song NN, Cheng X, Zhu L, Zhang Q, Zhang LL, et al. ZC4H2 stabilizes RNF220 to pattern ventral spinal cord through modulating Shh/Gli signaling. J Mol Cell Biol 2020; 12: 337-344.

8. Ma P, An T, Zhu L, Zhang L, Wang H, Ren B, et al. RNF220 is required for cerebellum development and regulates medulloblastoma progression through epigenetic modulation of Shh signaling. Development 2020b; 147: dev188078.

9. Zhang L, Ye M, Zhu L, Cha J, Li C, Yao YG, et al. Loss of ZC4H2 and RNF220 Inhibits Neural Stem Cell Proliferation and Promotes Neuronal Differentiation. Cells 2020; 9: 1600

10. Song NN, Ma P, Zhang Q, Zhang L, Wang H, Zhang L, et al. Rnf220/Zc4h2-mediated monoubiquitylation of Phox2 is required for noradrenergic neuron development. Development 2020 (Cambridge, England), 147, dev185199.

11. Padiath QS, Saigoh K, Schiffmann R, Asahara H, Yamada T, Koeppen A, et al. Lamin B1 duplications cause autosomal dominant leukodystrophy. Nat Genet 2006; 38: 1114-1123.

12. Giorgio E, Robyr D, Spielmann M, Ferrero E, Di Gregorio E, Imperiale D, et al. A large genomic deletion leads to enhancer adoption by the lamin B1 gene: a second path to autosomal dominant adult-onset demyelinating leukodystrophy (ADLD). Human Molecular Genetics 2015; 24: 3143–3154.

13. Compagnucci C, Piermarini E, Sferra A, Borghi R, Niceforo A, Petrini S, et al. Cytoskeletal dynamics during in vitro neurogenesis of induced pluripotent stem cells (iPSCs). Mol Cell Neurosci 2016; 77:113-124.

14. Dignam JD, Lebovitz RM, Roeder RG. Accurate transcription initiation by RNA polymerase II in a soluble extract from isolated mammalian nuclei. Nucleic Acids Res 1983; 11: 1475-1489.

15. Randles KN, Lam le T, Sewry CA, Puckelwartz M, Furling D, Wehnert M, et al. Nesprins, but not sun proteins, switch isoforms at the nuclear envelope during muscle development. Dev Dyn 2010; 239 :998-1009.

16. Karczewski KJ, Francioli LC, Tiao G, Cummings BB, Alföldi J, Wang Q, et al. The mutational constraint spectrum quantified from variation in 141,456 humans. Nature 2020; 581: 434-443.

17. Wiel L, Baakman C, Gilissen D, Veltman JA, Vriend G, Gilissen C. MetaDome: Pathogenicity analysis of genetic variants through aggregation of homologous human protein domains. Hum Mutat 2019; 40: 1030-1038.

18. Leuzzi V, Rinna A, Gallucci M, Di Capua M, Dionisi-Vici C, Longo D, et al. Ataxia, deafness, leukodystrophy: inherited disorder of the white matter in three related patients. Neurology 2000; 54: 2325-2328.

19. Lamond AI, Spector DL. Nuclear speckles: a model for nuclear organelles. [Review]. Nat Rev Mol Cell Biol 2003; 4: 605-612.

20. Rockel TD, Stuhlmann D, von Mikecz A. Proteasomes degrade proteins in focal subdomains of the human cell nucleus. J Cell Sci 2005; 118: 5231-5242.

21. Lallemand-Breitenbach V, Zhu J, Puvion F, Koken M, Honoré N, Doubeikovsky A, et al. Role of promyelocytic leukemia (PML) sumolation in nuclear body formation, 11S proteasome recruitment, and As2O3-induced PML or PML/retinoic acid receptor alpha degradation. J Exp Med 2001; 193: 1361-1371.

22. Janer A, Martin E, Muriel MP, Latouche M, Fujigasaki H, Ruberg M, et al. PML clastosomes prevent nuclear accumulation of mutant ataxin-7 and other polyglutamine proteins. J Cell Biol 2006; 174: 65-76.

23. Blank M. Targeted Regulation of Nuclear Lamins by Ubiquitin and Ubiquitin-Like Modifiers. Cells. 2020; 9:1340.

24. Dou Z, Xu C, Donahue G, Shimi T, Pan JA, Zhu J et al. Autophagy mediates degradation of nuclear lamina. Nature 2015; 527: 105-109.

25. Melberg A, Hallberg L, Kalimo H, Raininko R. MR characteristics and neuropathology in adult-onset autosomal dominant leukodystrophy with autonomic symptoms. AJNR Am J Neuroradiol 2006; 27: 904–911

26. Ciechanover A. The unravelling of the ubiquitin system. [Review]. Nat Rev Mol Cell Biol 2015; 16: 322-324.

27. Rousseau A, Bertolotti A. Regulation of proteasome assembly and activity in health and disease. [Review]. Nat Rev Mol Cell Biol 2018; 19697-19712.

28. Okamoto Y, Ozaki T, Miyazaki K, Aoyama M, Miyazaki M, Nakagawara A. UbcH10 is the cancer-related E2 ubiquitin-conjugating enzyme. Cancer Res 2003; 63: 4167-73.

29. Dhananjayan SC, Ismail A, Nawaz Z. Ubiquitin and control of transcription. [Review]. Essays Biochem 2005; 41: 69–80

30. von Mikecz A. The nuclear ubiquitin-proteasome system. [Review]. J Cell Sci 2006; 119: 1977-1984.

31. Rotin D, Kumar S. Physiological functions of the HECT family of ubiquitin ligases. [Review]. Nat Rev Mol Cell Biol 2009; 10: 398-409.

32. Dechat T, Gesson K, Foisner R. Lamina-independent lamins in the nuclear interior serve important functions. [Review]. Cold Spring Harb Symp Quant Biol 2010; 75: 533-543.

33. Prokocimer M, Barkan R, Gruenbaum Y. Hutchinson-Gilford progeria syndrome through the lens of transcription. [Review]. Aging Cell 2013; 12: 533-543.

34. Moir RD, Spann TP, Herrmann H, Goldman RD. Disruption of nuclear lamin organization blocks the elongation phase of DNA replication. J Cell Biol 2000; 149: 1179-92.

35. Manju K, Muralikrishna B, Parnaik VK. Expression of disease-causing lamin A mutants impairs the formation of DNA repair foci. J Cell Sci 2006; 119: 2704-2714.

36. Shimi T, Pfleghaar K, Kojima S, Pack CG, Solovei I, Goldman AE, et al. The A- and B-type nuclear laminnetworks: microdomains involved in chromatin organization and transcription. Genes Dev 2008; 15; 22: 3409-3421.

37. Dechat T, Adam SA, Goldman RD. Nuclear lamins and chromatin: when structure meets function. [Review]. Adv Enzyme Regul 2009; 49: 157-166.

38. Brunet A, Forsberg F, Fan Q, Sæther T, Collas P. Nuclear Lamin B1 Interactions With Chromatin During the Circadian Cycle Are Uncoupled From Periodic Gene Expression. Front Genet. 2019; 10: 917.

39. Earle AJ, Kirby TJ, Fedorchak GR, Isermann P, Patel J, Iruvanti S, et al.. Mutant lamins cause nuclear envelope rupture and DNA damage in skeletal muscle cells. Nat Mater 2020; 19: 464-473.

40. Ulianov SV, Doronin SA, Khrameeva EE, Kos PI, Luzhin AV, Starikov SS, et al. Nuclear lamina integrity is required for proper spatial organization of chromatin in Drosophila. Nat Commun 2019; 12; 10:1176.

41. Vergnes L, Péterfy M, Bergo MO, Young SG, Reue K. Lamin B1 is required for mouse development and nuclear integrity. Proc Natl Acad Sci U S A 2004; 101: 10428-33.

42. Coffinier C, Jung HJ, Nobumori C, Chang S, Tu Y, Barnes RH 2nd, et al. Deficiencies in lamin B1 and lamin B2 cause neurodevelopmental defects and distinct nuclear shape abnormalities in neurons. Mol Biol Cell 2011; 22: 4683-4693.

43. Lee JM, Tu Y, Tatar A, Wu D, Nobumori C, Jung HJ, et al. Reciprocal knock-in mice to investigate the functional redundancy of lamin B1 and lamin B2. Mol Biol Cell 2014; 25: 1666-1675.

44. Young SG, Jung HJ, Lee JM, Fong LG. Nuclear lamins and neurobiology. [Review]. Mol Cell Biol 2014; 34 : 2776-2785.

45. Chen NY, Yang Y, Weston TA, Belling JN, Heizer P, Tu Y, et al. An absence of lamin B1 in migrating neurons causes nuclear membrane ruptures and cell death. Proc Natl Acad Sci U S A 2019;116 : 25870-25879.

46. Brussino A, Vaula G, Cagnoli C, Panza E, Seri M, Di Gregorio E, et al. A family with autosomal dominant leukodystrophy linked to 5q23.2-q23.3 without lamin B1 mutations. Eur J Neurol 2010; 17: 541-549.

47. Barascu A, Le Chalony C, Pennarun G, Genet D, Imam N, Lopez B, et al. Oxidative stress induces an ATM-independent senescence pathway through p38 MAPK-mediated lamin B1 accumulation. EMBO J 2012; 31: 1080-94.

48. Barascu A, Le Chalony C, Pennarun G, Genet D, Zaarour N, Bertrand P. Oxydative stress alters nuclear shape through lamins dysregulation: a route to senescence. Nucleus 2012b; 3: 411-7.

49. Molloy A, Cotter O, van Spaendonk R, Sistermans E, Sweeney B. A patient with a rare leukodystrophy related to lamin B1 duplication. Ir Med J 2012; 105: 186-187.

50. Dai Y, Ma Y, Li S, Banerjee S, Liang S, Liu Q, et al. An LMNB1 Duplication Caused Adult-Onset Autosomal Dominant Leukodystrophy in Chinese Family: Clinical Manifestations, Neuroradiology and Genetic Diagnosis. Front Mol Neurosci 2017; 10: 215.

51. Mezaki N, Miura T, Ogaki K, Eriguchi M, Mizuno Y, Komatsu K, et al. Duplication and deletion upstream of LMNB1 in autosomal dominant adult-onset leukodystrophy. Neurol Genet 2018; 4: e292.

52. Pierce T, Worman HJ, Holy J. Neuronal differentiation of NT2/D1 teratocarcinoma cells is accompanied by a loss of lamin A/C expression and an increase in lamin B1 expression. Exp Neurol 1999; 157: 241-250.

53. Lin ST, Fu YH. miR-23 regulation of lamin B1 is crucial for oligodendrocyte development and myelination. Dis Model Mech 2009; 2: 178-188.

54. Lin ST, Huang Y, Zhang L, Heng MY, Ptácek LJ, Fu YH. MicroRNA-23a promotes myelination in the central nervous system. Proc Natl Acad Sci U S A 2013; 110: 17468-73.

55. Lin ST, Heng MY, Ptáček LJ, Fu YH. Regulation of Myelination in the Central Nervous System by Nuclear Lamin B1 and Non-coding RNAs. Transl Neurodegener 2014; 3:4.

56. Heng MY, Lin ST, Verret L, Huang Y, Kamiya S, Padiath QS, et al. Lamin B1 mediates cell-autonomous neuropathology in a leukodystrophy mouse model. J Clin Invest 2013; 123: 2719-2729.

57. Rolyan H, Tyurina YY, Hernandez M, Amoscato AA, Sparvero LJ, Nmezi BC, et al. Defects of Lipid Synthesis Are Linked to the Age-Dependent Demyelination Caused by Lamin B1 Overexpression. J Neurosci 2015; 35: 12002-1217.

58. Giacomini C, Mahajani S, Ruffilli R, Marotta R, Gasparini L. Lamin B1 protein is required for dendrite development in primary mouse cortical neurons. Mol Biol Cell 2016; 27: 35-47.

58. Yattah C, Hernandez M, Huang D, Park H, Liao W, Casaccia P. Dynamic Lamin B1-Gene Association During Oligodendrocyte Progenitor Differentiation. Neurochem Res 2020; 45: 606-619.

59. Takamori Y, Tamura Y, Kataoka Y, Cui Y, Seo S, Kanazawa T, et al. Differential expression of nuclear lamin, the major component of nuclear lamina, during neurogenesis in two germinal regions of adult rat brain. Eur J Neurosci 2007; 25:1653-1662.

60. Mahajani S, Giacomini C, Marinaro F, De Pietri D, Tonelli D, Contestabile A, et al. Lamin B1 levels modulate differentiation into neurons during embryonic corticogenesis. Sci Rep 2017; 7: 4897.

61. Khanna R, Krishnamoorthy V, Parnaik VK. E3 ubiquitin ligase RNF123 targets lamin B1 and lamin-binding proteins. FEBS J 2018; 285: 2243-62

62. Krishnamoorthy V, Khanna R, Parnaik VK. E3 ubiquitin ligase HECW2 targets PCNA and lamin B1. Biochim Biophys Acta Mol Cell Res 2018; 1865: 1088-1104.

63. Zhen R, Moo C, Zhao Z, Chen M, Feng H, Zheng X, et al. Wdr26 regulates nuclear condensation in developing erythroblasts. Blood 2020; 135: 208-219.

64. Peretto G, Di Resta C, Perversi J, Forleo C, Maggi L, Politano L, et al. Cardiac and Neuromuscular Features of Patients With LMNA-Related Cardiomyopathy. Ann Intern Med 2019; 171: 458-463.

65. Crasto S, My I, Di Pasquale E. The Broad Spectrum of LMNA Cardiac Diseases: From Molecular Mechanisms to Clinical Phenotype. [Review]. Front Physiol 2020; 11:761.

66. Sheikh FN, Hassan SA, Alam D, Kundi M, Hassan M. Lamin A/C Cardiomyopathy with E203K Pathogenic Mutation. Cureus 2020; 12: e7761.

67. Lattanzi G, Maggi L, Araujo-Vilar D. Laminopathies. Nucleus 2018; 9: 543-544.

68. Muchir A, Massart C, van Engelen BG, Lammens M, Bonne G, Worman HJ. Proteasome-mediated degradation of integral inner nuclear membrane protein emerin in fibroblasts lacking A-type lamins. Biochem Biophys Res Commun 2006; 351: 1011-1017.

69. Chaturvedi P, Parnaik VK. Lamin A rod domain mutants target heterochromatin protein 1alpha and beta for proteasomal degradation by activation of F-box protein, FBXW10. PLoS One 2010; 5: e10620.

70. Parnaik VK, Chaturvedi P, Muralikrishna B. Lamins, laminopathies and disease mechanisms: possible role for proteasomal degradation of key regulatory proteins. [Review]. J Biosci 2011; 36: 471-479.

71. Johnson BR, Nitta RT, Frock RL, Mounkes L, Barbie DA, Stewart CL, et al. A-type lamins regulate retinoblastoma protein function by promoting subnuclear localization and preventing proteasomal degradation. Proc Natl Acad Sci U S A 2004; 101: 9677-82.

72. Chaturvedi P, Khanna R, Parnaik VK. Ubiquitin ligase RNF123 mediates degradation of heterochromatin protein 1α and β in lamin A/C knock-down cells. PLoS One 2012; 7: e47558.

73. Buchwalter A, Schulte R, Tsai H, Capitanio J, Hetzer M. Selective clearance of the inner nuclear membrane protein emerin by vesicular transport during ER stress. Elife 2019; 8: e49796.

74. Koch B, Yu HG. Regulation of inner nuclear membrane associated protein degradation. Nucleus 2019; 10: 169-180.

75. Muralikrishna B, Chaturvedi P, Sinha K, Parnaik VK. Lamin misexpression upregulates three distinct ubiquitin ligase systems that degrade ATR kinase in HeLa cells. Mol Cell Biochem 2012; 365: 323-32.

76. Horn HF, Brownstein Z, Lenz DR, Shivatzki S, Dror AA, Dagan-Rosenfeld O, et al. The LINC complex is essential for hearing. J Clin Invest 2013; 123: 740-750.

77. Masterson J, Yıldırım B, Gökkaya E, Tokgöz Yılmaz S, Tekin M. A Novel Variant in SYNE4 Confirms its Causative Role in Sensorineural Hearing Loss. Balkan Med J 2018; 35: 196-198.

78. Tan KL, Haelterman NA, Kwartler CS, Regalado ES, Lee PT, Nagarkar-Jaiswal S, et al. Ari-1 Regulates Myonuclear Organization Together with Parkin and Is Associated with Aortic Aneurysms. Dev Cell 2018; 45: 226-244.e8.

79. Motta M, Pannone L, Pantaleoni F, Bocchinfuso G, Radio FC, Cecchetti S, et al. Enhanced MAPK1 Function Causes a Neurodevelopmental Disorder within the RASopathy Clinical Spectrum. Am J Hum Genet 2020; 107: 499-513.

80. Flex E, Martinelli S, Van Dijck A, Ciolfi A, Cecchetti S, Coluzzi E et al.. Aberrant Function of the C-Terminal Tail of HIST1H1E Accelerates Cellular Senescence and Causes Premature Aging. Am J Hum Genet 2019; 105: 493-508.

81. Van der Auwera GA, Carneiro M, Hartl C, Poplin R, del Angel G, Levy-Moonshine A, et al. From FastQ Data to High-Confidence Variant Calls: The Genome Analysis Toolkit Best Practices Pipeline. Curr Protoc Bioinformatics 2013; 43: 11.10.1-11.10.33

82. Cingolani P, Platts A, Wang le L, Coon M, Nguyen T, Wang L, et al. A program for annotating and predicting the effects of single nucleotide polymorphisms, SnpEff: SNPs in the genome of Drosophila melanogaster strain w1118; iso-2; iso-3. Fly 2012; 6: 80-92.

83. Liu X, Jian X, Boerwinkle E. dbNSFP v2.0: a database of human nonsynonymous SNVs and their functional predictions and annotations. Hum Mutat 2013; 34: E2393-2402.

84. Kircher M, Witten DM, Jain P, O'Roak, BJ, Cooper GM, Shendure J. A general framework for estimating the relative pathogenicity of human genetic variants. Nat Genet 2014; 46: 310-315.

85. Jagadeesh K, Wenger A, Berger M, Guturu H, Stenson P, Cooper D et al. M-CAP eliminates a majority of variants with uncertain significance in clinical exomes at high sensitivity. Nat Genet 2016; 48: 1581-1586.

86. Li Q, Wang K. InterVar: Clinical Interpretation of Genetic Variants by the 2015 ACMG-AMP Guidelines. Am J Hum Genet 2017; 100: 267-280.

87. Pieroni L, Finamore F, Ronci M, Mattoscio D, Marzano V, Mortera SL, et al. Proteomics investigation of human platelets in healthy donors and cystic fibrosis patients by shotgun nUPLC-MSE and 2DE: a comparative study. Mol Biosyst 2011; 7: 630–639.

88. Pieroni L, Levi Mortera S, Greco V, Sirolli V, Ronci M, Felaco P, et al. Biocompatibility assessment of haemodialysis membrane materials by proteomic investigations. Mol Biosyst 2015; 11: 1633–1643.

89. Terracciano A, Casali C, Grieco GS, Orteschi D, Di Giandomenico S, Seminara L et al. An inherited large-scale rearrangement in SACS associated with spastic ataxia and hearing loss. Neurogenetics. 2009 ;10:151-155.

90. Seelow D, Schuelke M, Hildebrandt F, Nürnberg P. HomozygosityMapper--an interactive approach to homozygosity mapping. Nucleic Acids Res 2009;37(Web Server issue):W593-99.

Figure legends

Figure 1A and B. Fig 1A. Pedigrees of the families. Pedigree1# is reported in Leuzzi *et al.*, 2000. **Fig.1B. Multiple sequence alignment of RNF220 proteins.** Multiple sequence alignment of RNF220 proteins (ClustalW) from different organisms around the sites affected

by AR-LAD mutations R363Q and R365Q (in red). "*" indicates perfect conservation ,":" indicates strong similarity, "." indicates weak similarity.

Figure 2. MRI characteristics of AR-LAD. A-E, and I: pedigree 4, Pt II,1 at age 7; F-H: pedigree 3, Pt I,3 at age 7y; J-L: pedigree 1, Pt 3 at age 7y. Images demonstrate very similar findings: T2 weighted image are A-C, E, F-K, show diffuse T2 hyperintensity in the white matter of the brain suggesting a hypomyelinating leukoencephalopathy.T2 hyperintense areas were particularly enhanced at the level of the periventricular white matter areas (arrows). Note the normal myelination of cerebellar white matter in I and K, and the global corpus callosum thinning on T1 weighted image (D, L).

Figure 3. RNF220 immunohistochemical detection in the CNS of a 8 day-old mice. Significant expression of RNF220 is observed in the molecular layer of hippocampus, in telencephalon, with a conspicuous signal in the cerebellum. Upper panel) Sagittal brain sections from 8 day-old mouse were stained for RNF220 in combination with the neural markers Smi32 and Calbindin, and astro-glial marker GFAP. Nuclei were counterstained with Hoechst (Scale bar=100μm). Inserts are magnifications of the selected areas. (Scale bar= 25μm). Lower panel) Higher magnification of sagittal cerebellum sections from 8 day-old mice labelled for RNF220 in combination with the neuronal markers Smi32 and Calbindin. Nuclei were counterstained with Hoechst (Scale bar= 25μm).

Figure 4. RNF220 subcellular localization in COS-1 cells at different times of transfections and RNF220 and 20S-proteasome subcellular localizations in AR-LAD primary fibroblasts. A) Left panel. COS-1 cells transfected using 1 ug of FLAG-tagged RNF220 (wild-type or mutants) were immunostained with the anti-FLAG antibody and Hoechst, after 24 hours of transfection (Scale bar= 25μm). Bar graph indicates the frequency of nuclear and cytosolic localization of RNF220 (wild type and mutants). Results are presented as mean ± SEM (n=123 cells from WT, 141 cells from R363Q, 135 cells from R365Q). Student's t-test, ** $p \leq 0.01$**. Right panel.** COS-1 cells expressing FLAG-tagged RNF220 (wild-type or mutants) were immunostained with the anti-FLAG antibody and Hoechst, after 48 hours of transfection (Scale bar= 25μm). Results are presented as mean ± SEM (n=150 cells from WT, 123 cells from R363Q, 137 cells from R365Q). Student's t-test, * $p \leq 0.05$, ** $p \leq 0.01$**. B) Left panel.** Primary fibroblasts obtained from healthy (Ctrl) and AR-LAD patients were immunostained with the anti RNF220 antibody and Hoechsts (Scale bar= 25μm).AR-LAD fibroblasts showed a preferential cytosolic localization of RNF220, as compared to control fibroblasts. **Right panel.** Primary fibroblastst obtained from healthy and

AR-LAD patients were immunostained with the anti 20Sproteasome antibody and Hoechsts (Scale bar= 25μm). In control fibroblasts the 20S-proteasome presents a nuclear diffuse distribution. In AR-LAD fibroblasts harbouring the p.R365Q substitution the 20Sproteasome forms cytosolic aggregate, suggesting a flooding of the overall proteolytic capacity. In AR-LAD cells harboring the p.R363Q mutation, nuclear aggregates of the 20S-proteasome are observed.

Figure 5. Effects of RNAi-mediated downregulation of RNF220 Drosophila orthologue in different fly tissues. A) Expression in fly muscle of a specific RNAi construct that targets fly RNF220, under control *MEF2*-GAL4 driver, at 25°C, caused adult fly lethality. Total RNA extracted from fly larvae expressing UAS-RNF220-RNAi under *MEF2*-GAL4, or the driver alone, was analyzed by qRT-PCR. Relative levels of RNF220 transcript between genotypes are shown. SEM was calculated from n = 3 independent experiments. * = P <0.05. B) RNAi-mediated downregulation of RNF220 significantly affects fly eye development. Flies expressing RNF220 RNAi construct late during eye development, under GMR-GAL4, show strong retina degeneration at 25 °C (upper panels). Expression of the same RNAi construct early during eye development, under *eyeless*-GAL4, causes fly lethality at 25°C. Flies grown at 18 °C show severe alterations of eye morphology and a significant reduction of eye surface (lower panels). C) RNAi repression of RNF220 in larval salivary glands strongly affects the subcellular localization of Lamin Dm0 and promotes its accumulation. Salivary gland cells were dissect from fly larvae expressing UAS-RNF220-RNAi under *eyeless*-GAL4, or *eyeless*-GAL4 on its own, and were stained in immunofluorescence experiments with antibodies against Lamin Dm0. Different rates of accumulation of lamin Dm0 and the different kinds of protein aggregate are shown. D) Immunofluorescence labeling with antibodies against Lamin C of cells from the same genotypes were used as control (Scale bars = 10μm).

Figure 6 A and B. Fig. 6A. Co-immunoprecipitation of lamin B1 and RNF220 from cerebellum extract showing tight link between RNF220 and lamin B1. Proteins in RIPA buffer were immunoprecipitated with anti-Lamin B1 antibody or mouse IgG, as negative control. Proteins retained on the beads were separated by SDS-PAGE and analyzed by Western blotting with corresponding antibodies. Loaded 1:50 of extract utilized for each immunoprecipitation as starting material (SM), and 1:2 of bound proteins as immunoprecipitated material (IP). Western blotting signals of two independent experiments, normalized on the amount of IgG, were acquired by Fiji NIH ImgeJ software, and their

statistical significance was assessed using GraphPad Prism software (version 8.0) with one-way ANOVA analysis according to Sidak's multitple comparisons test. p<0,01**;p<0,001*** (Left graph). Fig. 6B. RNF220 interacts with proteins of nuclear lamina. Effect of p.R363Q and p.R365Q substitution on RNF220 binding activity for Lamin B1. The nuclear fraction of HEK-293T cells expressing FLAG-tagged RNF220 (wild type or mutants) were subjected to immunoprecipitation experiments using the anti-FLAG monoclonal antibody covalently attached to sepharose beads to detect the interaction between RNF220 and endogenous Lamin B1. Both R363Q and R365Q substitutions show reduced binding to lamin B1 compared to WT RNF220, when the amount of lamin B1-bound is normalized for the level of RNF220 pulled down. The graph reports densitometric quantification of Lamin B1 retained by each RNF220 protein variant. Results are presented as mean ± SEM. n =3, Student's t-test,* $p \leq 0.05$.

Figure7. RNF220 mutations affect nuclear envelop integrity by altering Lamin and Nesprin localization in AR-LAD fibroblasts. Primary fibroblasts of healthy (Ctrl) and AR-LAD affected (R363Q and R365Q) individuals were labelled with Lamin B1, Lamin A/C and Nesprin 1 antibodies and counterstained with Hoechst (Scale bar=25µm). Nuclear envelop of AR-LAD fibroblasts show abnormal invaginations and lobulations and increased levels of all markers (lamin B1 A/C and Nesprin1). Bar graph indicates the frequency of cells with nuclear envelope defects and irregular nuclear margins. Results are presented as the mean ± SEM (n=251 cells from WT, 177 from R363Q, 186 cells from R365Q). Student's t-test, **** $p \leq 0.001$, *** $p \leq 0.005$.
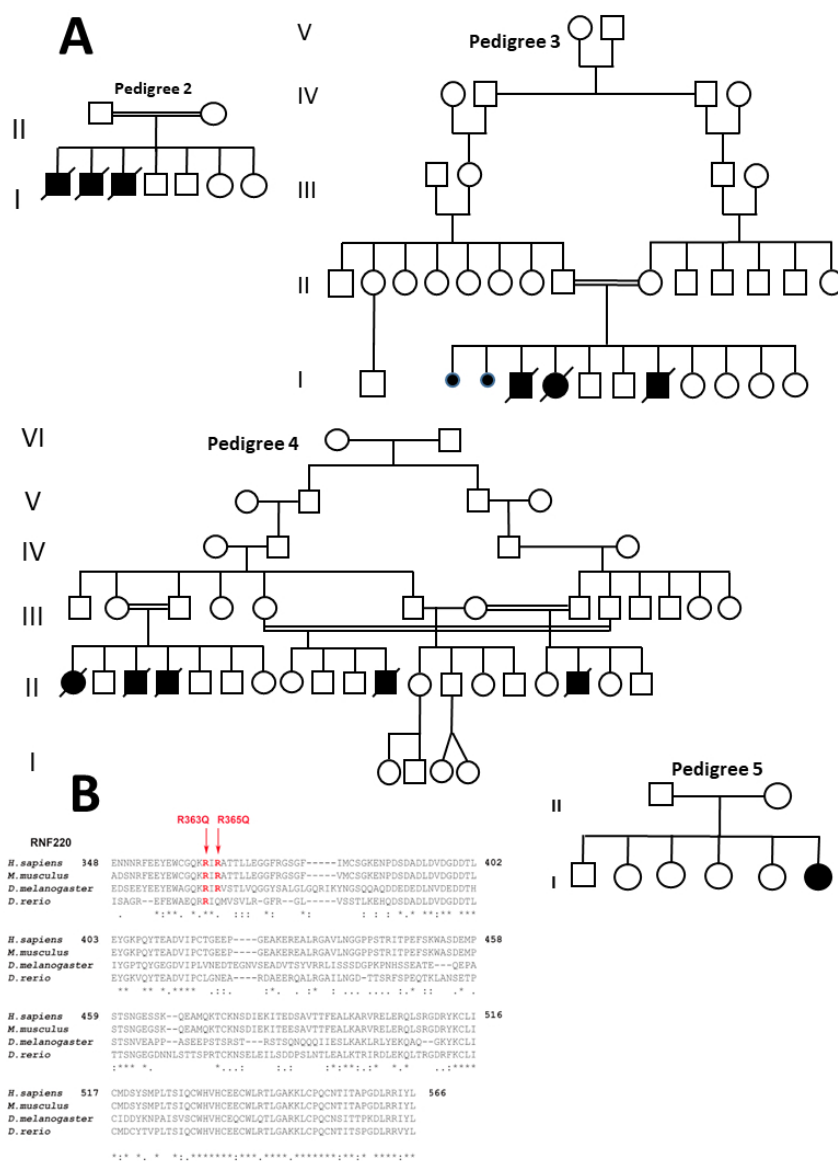
Figure 1A and B. Fig 1A. Pedigrees of the families.Fig.1B. Multiple sequence alignment of RNF220 proteins
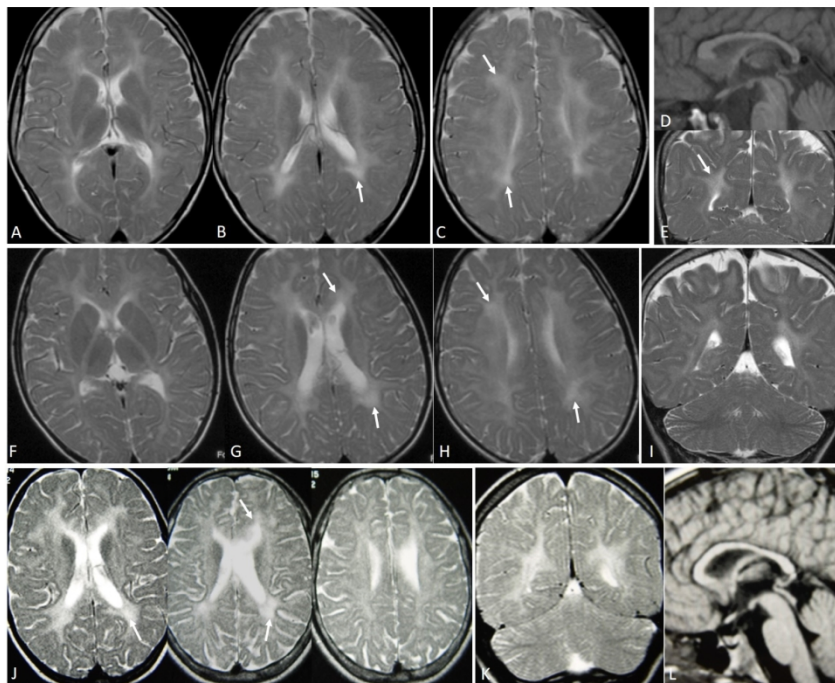
209x289mm (96 x 96 DPI)

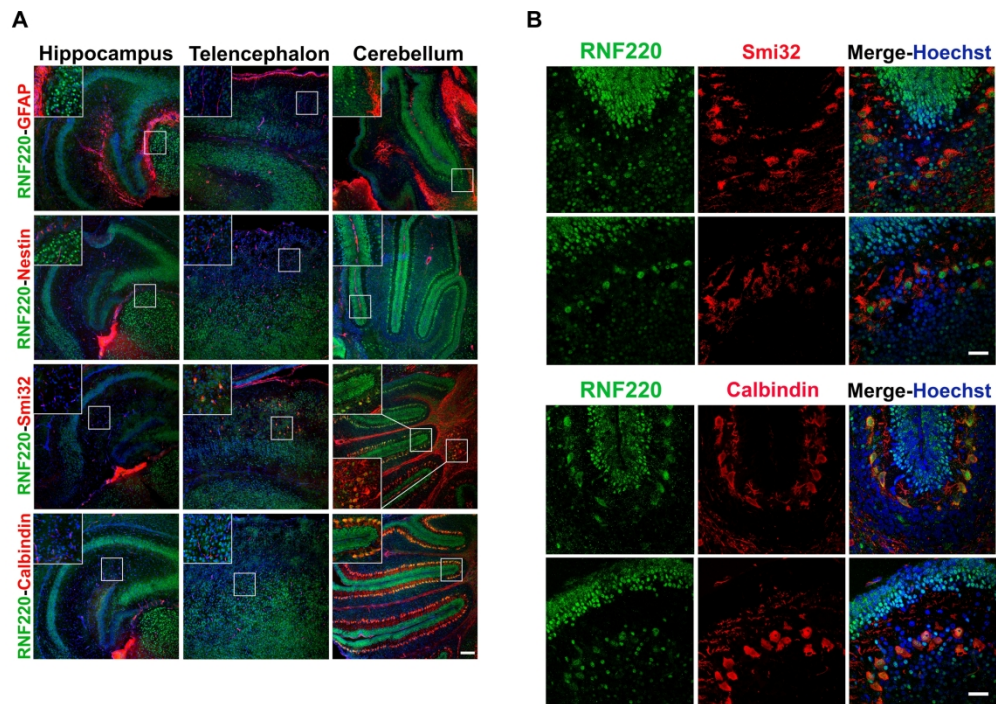Figure 2. MRI characteristics of AR-LAD

583x825mm (72 x 72 DPI)

Figure 3 RNF220 immunohistochemical detection in the CNS of a 8 day-old mice
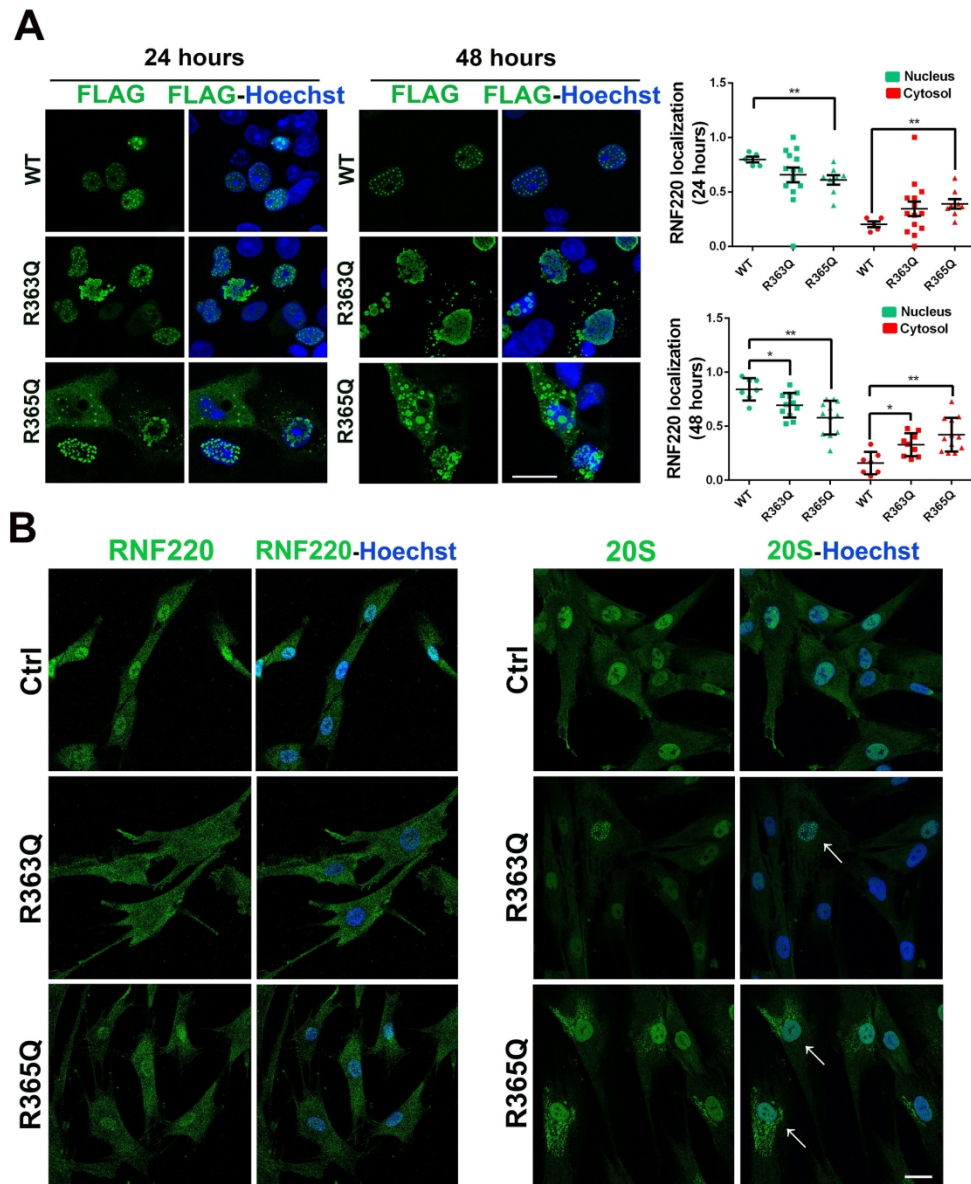
278x195mm (300 x 300 DPI)

Figure 4 RNF220 subcellular localization in COS-1 cells at different times of transfections and RNF220 and 20S-proteasome subcellular localizations in AR-LAD primary fibroblasts
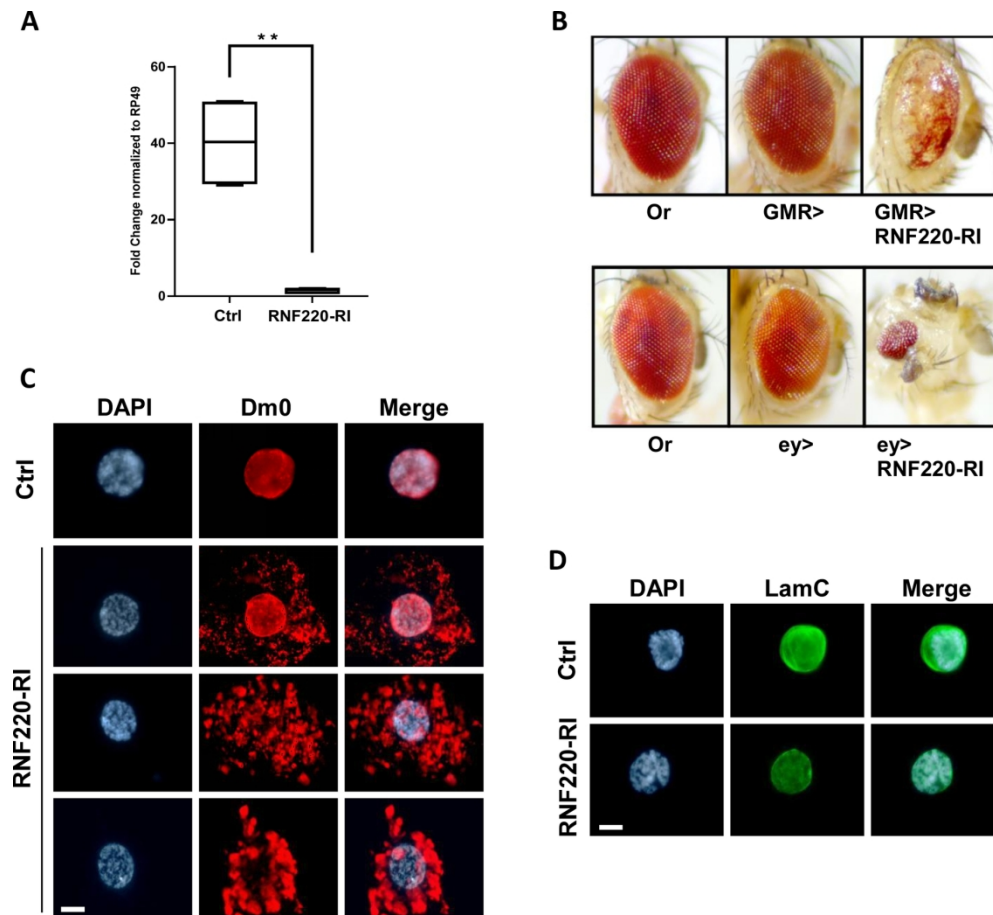
99x119mm (600 x 600 DPI)

Figure 5 Effects of RNAi-mediated downregulation of RNF220 Drosophila orthologue in different fly tissues
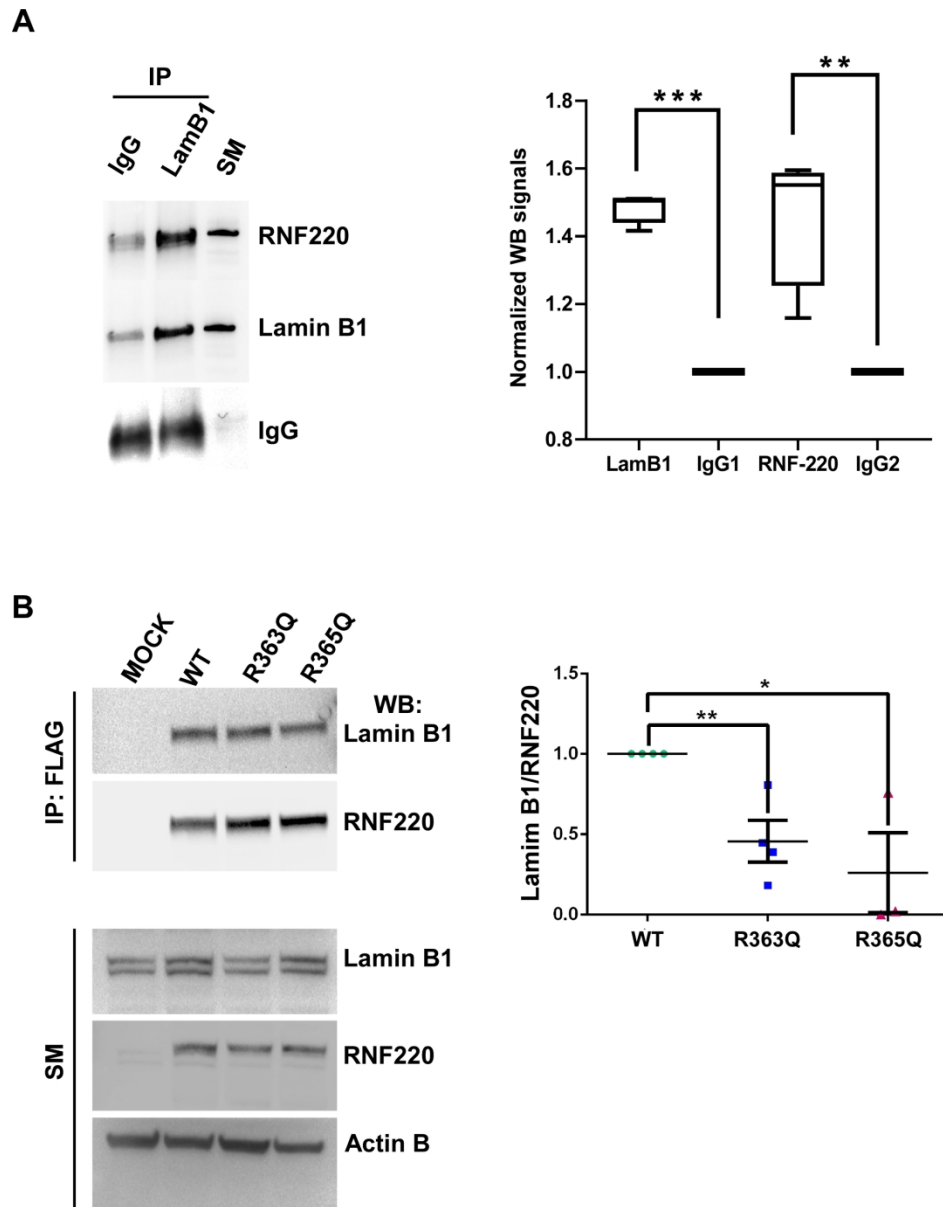
166x153mm (300 x 300 DPI)

Figure 6 Co-immunoprecipitation of lamin B1 and RNF from cerebellum extract showing tight link between RNF220 and lamin B1
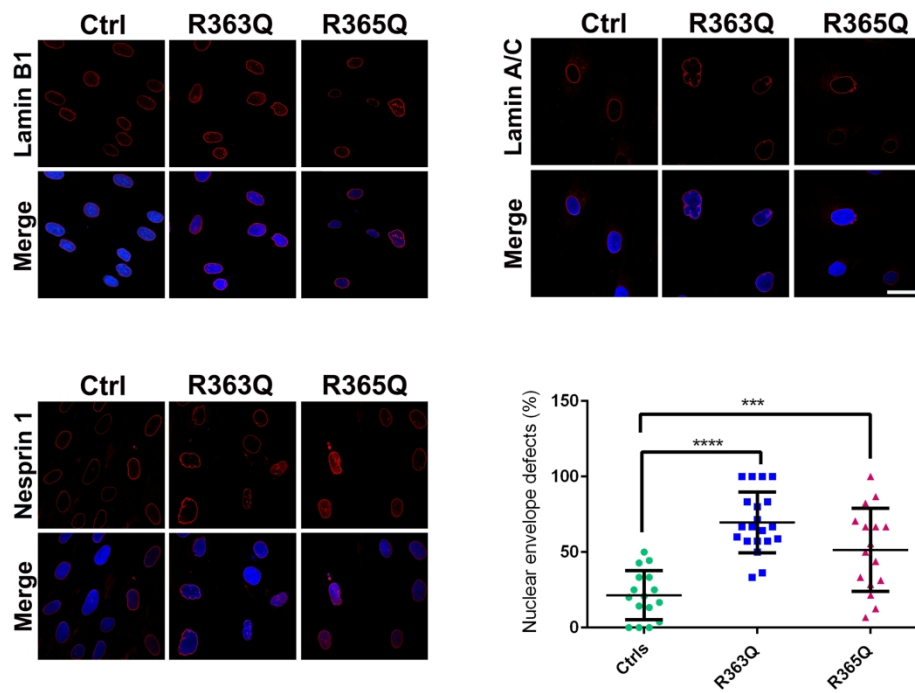
190x240mm (300 x 300 DPI)

Figure 7 RNF220 mutations affect nuclear envelop integrity by altering Lamin and Nesprin localization in AR-LAD fibroblasts

187x145mm (600 x 600 DPI)

Table 1. Details of Clinical Features

Patient ID	Pedigree 1; pt 1 (Leuzzi et al., 2000)	Pedigree 1; pt 2 (Leuzzi et al., 2000)	Pedigree 1; pt 3 (Leuzzi et al., 2000)	Pedigree 2, pt I,3	Pedigree 3, pt I,4	Pedigree 4, pt II,4	Pedigree 4, pt II,11	Pedigree 4, pt II, 17	Pedigree 5, pt I,6
Sex	F	M	F	M	M	M	M	M	F
death (age, y)	21	18	18	10	10	10	10	11	11
Ethnicity	Caucasian (Southern Italy)	Caucasian (Southern Italy)	Caucasian (Southern Italy)	Roma	Roma	Roma	Roma	Roma	Roma
RNF220 mutation	c. 1088G>A p.Arg363Gly homo	c. 1088G>A p.Arg363Gly homo	c. 1088G>A p.Arg363Gly homo	c.1094G>A p.Arg365Gly homo	c.1094G>A p.Arg365Gly homo	c.1094G>A p.Arg365Gly homo	c.1094G>A p.Arg365Gly homo	c.1094G>A p.Arg365Gly homo	c.1094G>A p.Arg365Gly homo
Birth parameters (l, w, ofc) - Centile	at term, w 3.200 gr (25°/50°/50°)	at term , w 3, 850 gr (75%ile) 50°/75°/50°	at term, w 3,000 gr 25°/50°/50°	at term w 3380 gr 50°/50°/50°	premature (33 weeks) w 2,010 gr 3°/3°/3°	At term w 3,420 gr 50°/50°/50°	At 39 week gestation, w 3,200 gr 25°/25°/50°	At term 3,450 gr 50°/50°/50°	36 weeks, w 3,120 gr 50°/50°/50°
Growth parameters (h, w, ofc) - Centile	at age of 7.3 yrs: w 21 kg (25%ile); h 121 cm (50%ile); ofc 50.5 (50%ile)	at the age of 7 yr: w 27 kg (90%ile); h 130 (90%ile) cm; ofc 57 (> 98%ile)	at age of 8 yr: w 52 kg (+3,05 SD); h137.4 cm (+1.2 SD); at age of 9 yr ofc 55 cm (+1,67 SD);	At age 5 months l: 61 cm (<3%); w: 6.2 kg (<3%); ofc: 40cm (>3%)	na	na	at 7.5 years: h (3%ile) ; w (50%ile); ofc(25% ile)	na	at age 7 years: h(50%ile); w(50%ile); ofc (50%ile)
Consanguinity	+	+	+	+	+	+	+	+	-
First symptoms (age in y, which)	developmental delay (mainly walking)	developmental delay (mainly walking)	developmental delay (mainly speech), mild intellectual disability	developmental delay (mainly speech), intellectual disability	developmental delay (walking and speech), intellectual disability	ataxia (5)	ataxia (5)	ataxia(3), cognitive deterioration	ataxia (4)
Neuropsychiatric manifestations									
Motor developmental delay	+	+	+	+	+	-	-	-	-
Intellectual disability (IQ)	-(78)	-(77)	+(59)	+	+(44)	-(85)	+	-	+(67)
Neurologic manifestations									
Ataxia(age at diagnosis, y)	+(3)	+(3)	+(1)	+(2)	+(2,5)	+(5)	+(5)	+(3)	+(4)
Spastic paraplegia (age)	+	+	+	+	+	+	+	+	+(10)
Hyperreflexia	+	+	+	+	+	+	+	+	
Dysarthria	+	+	+	+	+	+	+	+	+
Peripheral neuropathy (axonal)	-	-	+	+	+	+	+	-	-
Seizures/EEG abnormalities	-	-	-	-	-	-	-	+	-
Wheelchair-bound at age of (y)	13	16	17	9	9	9	9	8	8
Neuroimaging (MRI)									
Cerebellar atrophy	-	+	-	+	+	-	-	-	-
White matter involvement (hypomyelination)	+	+	+	+	+	+	+	+	+
Thin corpus callosum	+	+	+	+	+	+	+	+	+
Hepatic involvement									
age at onset (y)	3	4	3	3	8	7	5	5	n.a.
Elevated liver enzymes (age)	+(3)	+(4)	+(3)	+(3)	+(8)	+(8)	+(5)	+(5)	n.a.
Liver biopsy	-	-	-	+(hepatic fibrosis)	+(hepatic fibrosis)	-	-	+(hepatic fibrosis)	-
Ultrasonography (abnormal)	+	+	+	+	+	+	+	+	-
Heart Involvement									
dilated cardiomyopathy (age at onset, y)	+(18)	+(17)	+(15)	+(9)	+(10)	+(9)	+(9)	+(8)	+(10)
Deafness									
Sensorineural hearing loss (age at onset)	+(7)	+(9)	+(9)	+(9)	+(6)	+(8)	+(5)	+(7,5)	+(7)